

Communication

Synthesis and Crystal Structure of a Zn(II)-Based MOF Bearing Neutral N-Donor Linker and SiF_6^{2-} Anion

Biplab Manna ^{1,†}, Shivani Sharma ^{1,†} and Sujit K. Ghosh ^{1,2,*}

¹ Department of Chemistry, Indian Institute of Science Education and Research (IISER Pune), Dr. Homi Bhabha Road, Pashan, Pune 411008, India; biplabchem.manna@gmail.com (B.M.); shivani.sharma@students.iiserpune.ac.in (S.S.)

² Centre for Research in Energy & Sustainable Materials, IISER Pune, Dr. Homi Bhabha Road, Pashan, Pune 411008, India

* Correspondence: sghosh@iiserpune.ac.in; Tel.: +91-20-2590-8076

† These authors contributed equally to this work.

Received: 20 November 2017; Accepted: 10 January 2018; Published: 16 January 2018

Abstract: A novel three-dimensional two-fold interpenetrated bi-porous metal-organic framework IPM-325 (IPM: IISER Pune Materials) having **pcu** topology was synthesized at room temperature. Single crystal X-ray diffraction (SC-XRD) study revealed that the compound crystallizes in monoclinic lattice with molecular formula $[\text{Zn}(\text{L})_2(\text{SiF}_6)](\text{CH}_2\text{Cl}_2)_x\text{G}_n$ where G = Guests). All metal centers were found to have octahedral geometry. From single crystal analysis it can be inferred that SiF_6^{2-} anion play a vital role in extending the dimensionality of the framework by bridging between two metal centers. Interestingly, IPM-325 exhibited two-step structural transformation maintaining the crystallinity of the framework as characterized by powder X-ray diffraction (PXRD).

Keywords: metal-organic framework; neutral N-donor framework; structural transformations

1. Introduction

Metal-organic frameworks (MOFs)/Porous coordination polymers (PCPs) have shown immense potential in various domains including separation, storage, sensing, catalysis, etc. [1–5]. MOFs are extended networks constituting of metal nodes and organic moiety linked via coordination bonds resulting in framework formation with potential voids [6,7]. MOFs can be readily functionalized using different organic building blocks thus imparting flexibility to tune the properties [8]. Metal-organic frameworks can also be tuned by using varied metals/metal clusters along with counter ions with different coordinating tendency [9–13]. MOFs have been classified as neutral and ionic MOFs (iMOFs) based on the framework charge [14]. Among various type of linkers, neutral nitrogen donor-based linkers have played a vital role since the emergence of MOFs owing to the easy availability and facile coordinating ability [15,16]. In pioneering reports, Zaworotko and Kitagawa have reported MOFs utilizing SiF_6^{2-} as counter anion and neutral nitrogen donor linker [17,18]. Recently, (SiF_6^{2-}) anion has been utilized extensively due to the tendency of SiF_6^{2-} to bridge two-dimensional sheets to form an overall three-dimensional framework with formation of one dimensional channel with varied porosity depending on the length of the linker [19,20]. Owing to the presence of highly electronegative fluorine atoms in SiF_6^{2-} it leads to the formation of highly charged polar surfaces. Owing to the highly charged polar surfaces, SiF_6^{2-} anion based MOFs are currently being pursued in various sorption-based applications like CO_2 capture, water sorption, hydrocarbon separation, etc. [21–23]. Thus, SiF_6^{2-} as an inorganic pillar should be utilized to develop novel materials as it imparts higher selectivity in sorption-based applications.

Yet another important classification within the field of MOFs is to classify MOFs as rigid MOF or flexible MOF depending on the frameworks tendency to change the structure on the application of varied stimuli like pressure, temperature, etc. [24–26]. Flexible MOFs are the frameworks which tend to change the overall structure upon applications of different stimuli. Flexible MOFs have been utilized in various adsorption-based separation processes with promising results [27,28]. Thus, development of MOFs that exhibit structural transformation is quite crucial for the development of materials exhibiting selective sorption.

SiF_6^{2-} anion-based rigid MOFs have been extensively studied but less attention has been paid towards flexible SiF_6^{2-} -based MOF system. SiF_6^{2-} anion-based flexible MOFs may show dual facet of high selectivity, hysteretic sorption along with various characteristics of flexible MOFs accompanied with properties imparted by SiF_6^{2-} anions. Herein, we report the crystal structure of IPM-325 which exhibits structural transformations as characterized by PXRD.

2. Materials and Methods

All the starting reagents zinc hexafluorosilicate hydrate, (1*E*,2*E*)-1,2-bis(pyridin-4-ylmethylene)hydrazine were purchased from Sigma-Aldrich, Bangalore Karnataka, India and all the solvents were procured locally. Powder X-ray diffraction (PXRD) patterns were measured on Bruker D8 Advanced X-ray diffractometer (Bruker AXS GmbH, Karlsruhe, Germany) at room temperature using Cu-K α radiation ($\lambda = 1.5406 \text{ \AA}$) with a scan speed of $0.5^\circ \text{ min}^{-1}$ and a step size of 0.01° in 2θ . Thermogravimetric analysis results were obtained in the temperature range of 30–800 °C on Perkin-Elmer STA 6000 analyzer (TGA, STA 6000 Perkin Elmer, PerkinElmer, Inc., Waltham, MA, USA) under N_2 atmosphere, at a heating rate of $10^\circ \text{ C min}^{-1}$. Single-crystal X-ray data of IPM-325_P1 was collected at 100 K on a Bruker KAPPA APEX II CCD Duo diffractometer (operated at 1500 W power: 50 kV, 30 mA, Bruker AXS GmbH, Karlsruhe, Germany) using graphite-monochromated Mo K α radiation ($\lambda = 0.71073 \text{ \AA}$). A crystal was mounted on a nylon Cryoloop (Hampton Research) with Paratone-N oil (Hampton Research). The data integration and reduction were processed with SAINT software [29]. A multi-scan absorption correction was applied to the collected reflections [30]. The structure was solved by the direct method using SHELXS-2014 [31] and was refined on F_2 by full-matrix least-squares technique using the SHELXL-2017 [32] program package within the WINGX program [33]. All non-hydrogen atoms were refined anisotropically. All hydrogen atoms were located in successive difference Fourier maps and they were treated as riding atoms using SHELXL default parameters. Highly disordered guest solvent molecules were observed. SQUEEZE option was used that eliminate the contribution of disordered guest molecules [34]. Residual electron density was calculated from the SQUEEZE function 49 electrons/unit cell. Gas adsorption measurements were performed using BelSorp-Max instrument (BEL Japan, Inc., Osaka, Japan).

Experimental Synthesis

Synthesis of Linker L ((1*E*,2*E*)-1,2-bis(pyridin-4-ylmethylene)hydrazine): Linker L was synthesized by modifying a reported protocol [35]. 4-pyridinecarboxaldehyde (49.94 mmol, 4.704 mL) was taken in a round bottomed flask. To this flask (1:1) Methanol (15 mL) and ethanol (15 mL) solution was added and catalytic quantity of acetic acid was added to this mixture. This mixture was stirred at 120 °C for 0.5 h. Further, hydrazine hydrate (19.97 mmol, 0.970 mL) was added and the reaction was maintained at 120 °C for 12 h. Subsequent cooling to room temperature yielded yellow crystalline product. Crude product was recrystallized from a solvent combination of methanol: ethanol solvent mixture. Yield = 90%.

Synthesis of IPM-325_p1: Single crystals of IPM-325_p1 were obtained by slow diffusion 1:1 mixture of zinc hexafluorosilicate hydrate ($\text{ZnSiF}_6 \cdot \text{H}_2\text{O}$) (0.1 mmol, 20.7 mg) and L = (1*E*,2*E*)-1,2-bis(pyridin-4-ylmethylene)hydrazine (0.1 mmol, 21 mg) in a solvent combination of Dichloromethane, methanol and benzene. Block shaped yellow colored crystal was obtained after one week. Yield ~60%.

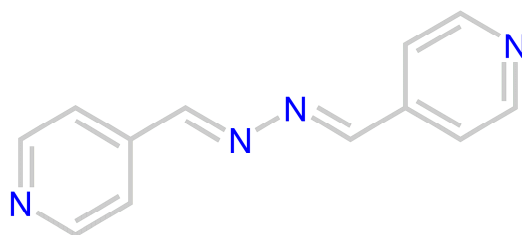
Desolvated phase preparation: IPM-325_p1 was heated at 160 °C overnight with slow increase in the temperature at the rate of 5 °C/h and then maintaining 160 °C overnight. The desolvated phase was further characterized by thermogravimetric analysis.

3. Results and Discussions

IPM-325 was synthesized by slow diffusion of ligand L (Scheme 1) and ZnSiF₆ at room temperature to yield block shaped yellow colored crystals. Single crystal X-ray diffraction analysis revealed that the compound crystallizes in *C2/m* space group with *Z* = 2 (Table 1). The asymmetric unit consist of Zn(II) metal ion along with two linkers and SiF₆²⁻ anion with dichloromethane molecules and other disordered molecules present within the voids (Figure 1). Zn(II) metal node is octahedrally coordinated with N₄F₂ donor set with the distance between Zn(II) and equatorial nitrogen atoms 2.139 Å while the distance between Zn(II) and axial F atoms was 2.153 Å. SiF₆²⁻ anions were found to bridge between two metal centers (Figure 2a). Overall structure was found to be two-fold interpenetrated in nature with an overall **pcu** topology (Figure 2b). Along the *a*-axis, the packing diagram showed types of rectangular voids Pore A and Pore B having dimensions 5.55 × 7.46 Å² and 5.84 × 6.54 Å² respectively (excluding van der Waals radii) (Figure 2b). The voids of the asynthesized framework (Figure 3) (IPM-325_p1; p represents phase) are filled with dichloromethane solvent wherein the H6 atom exhibits hydrogen bonding interaction with the F3 atom present at the metal node. To establish the bulk phase purity of IPM-325_p1, it was characterized using powder X-Ray diffraction measurements (PXRD) which showed a considerable shift in the observed pattern when compared to the simulated pattern (Figure 4a). The observed shift may be due to the overall structural transformation leading to formation of new phase named as IPM-325_p2 (p represents phase). To establish the bulk phase purity, we performed PXRD analysis of asynthesized crystals in presence of mother liquor. The PXRD pattern corroborated well with the simulated pattern (Figure 4a) thus establishing the bulk phase purity of IPM_325p1.

We observed a considerable shift in the PXRD pattern of the asynthesized compound upon exposure to air. This shift may be attributed to the sliding of the interpenetrated networks at ambient conditions due to escaping of low boiling guests from the voids. The PXRD profile showed an entirely new pattern thus confirming the formation of another structure. Another interesting observation from the PXRD pattern is that the intensity profile at 2θ = 5.37° peak exhibited a highly sharp peak after long exposure to ambient conditions. From this it can be inferred that IPM-325_p2 retains a crystalline nature after exposure to ambient conditions thus establishing the air stability of this phase. Due to the drastic shift observed in PXRD, we sought to obtain a single crystal of IPM-325_p2 after air exposure but due to the poor quality of the crystal we were unable to obtain single crystal data. Thermogravimetric analysis of the IPM-325_p2 present at ambient conditions showed ~10% weight loss around ~103 °C owing to the presence of occluded guests molecules present within the pores with overall loss of 20% observed until 220 °C. (Figure 4b). To obtain the desolvated phase of compound the material was heated at elevated temperature (160 °C) overnight with vacuum and further characterized via both PXRD and TGA measurements. Desolvated phase was characterized using thermogravimetric analysis which showed no initial loss in the desolvated phase of compound ~220 °C after which a gradual loss was observed which can be correlated to the decomposition of the framework. Powder X-ray diffraction measurement of the desolvated phase exhibited an entirely new pattern with the retention of original peak at 2θ = 5.37° along with the emergence of some new peaks (Figure 4a). Thus, IPM-325_p2 showed another structural transformation to yield the desolvated phase IPM-325_p3 (p represents phase). Also, the peak at 2θ = 5.37° maintained its intensity thus from which we can infer that the desolvated framework is highly crystalline in nature. Low temperature N₂ adsorption was performed, which revealed slow opening of the pore (Figure 5).

Thus, we have successfully synthesized and characterized a bi-porous MOF; IPM-325_p1 wherein SiF₆²⁻ anion acts as an inorganic pillar. IPM-325_p2 shows structural transformation as analyzed by PXRD measurements. Further investigations regarding the structural aspect of the desolvated phase IPM-325_p3 and its sorption measurements are currently being pursued in our lab.



Scheme 1. Chemical diagram of linker L = ((1E,2E)-1,2-bis(pyridin-4-ylmethylene)hydrazine).

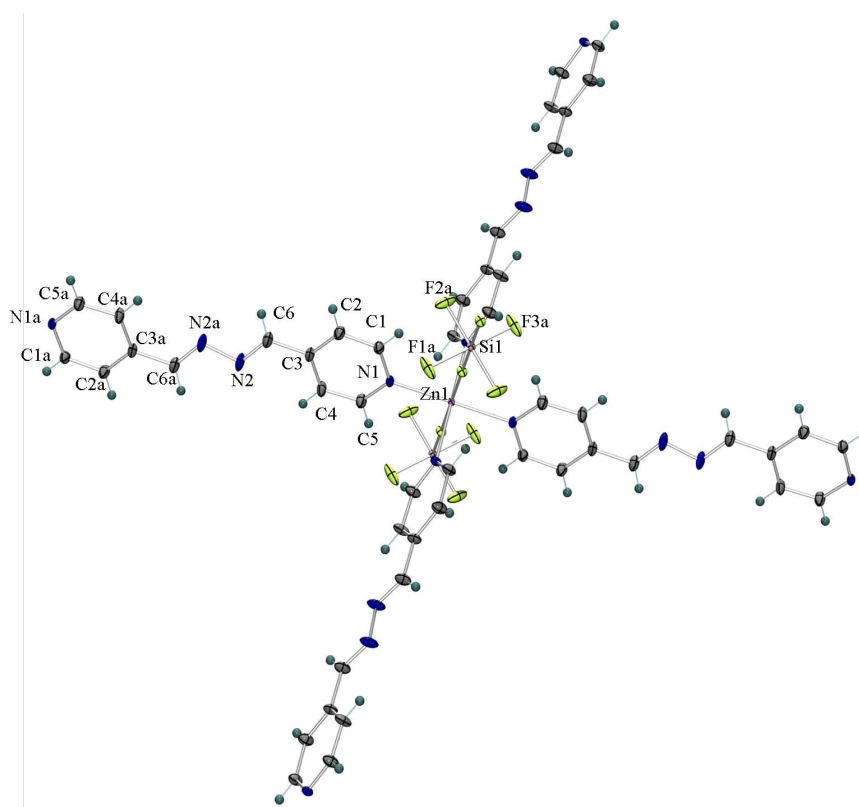


Figure 1. Ortep diagram showing coordination sphere around Zn(II) metal ion in thermal ellipsoids (50% probability).

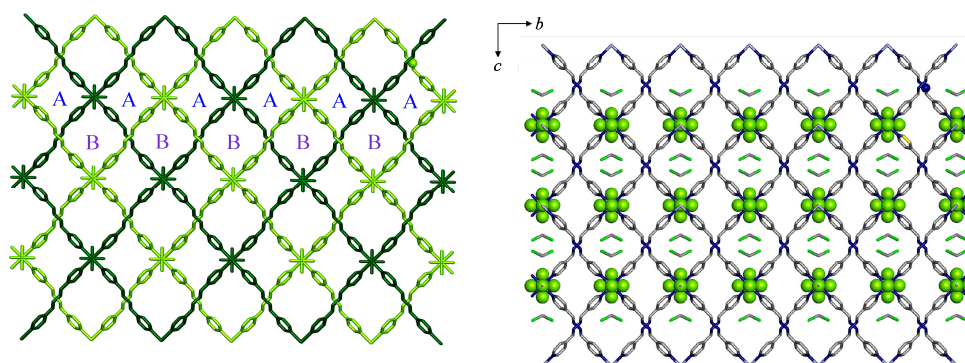


Figure 2. (a) Packing diagram along *a*-axis of IPM-325_p1 with guests solvent molecules present within the one-dimensional pore channel; (b) Packing diagram of IPM-325_p1 along *a*-axis depicting two-fold interpenetration along with two kinds of pore. (Hydrogen atoms have been omitted for clarity) Color: Grey—C, Light Blue—N, Dark Blue—Zn, Green—Fluorine, Red—Silicon, Light green—Chlorine. Solvent hidden for clarity.

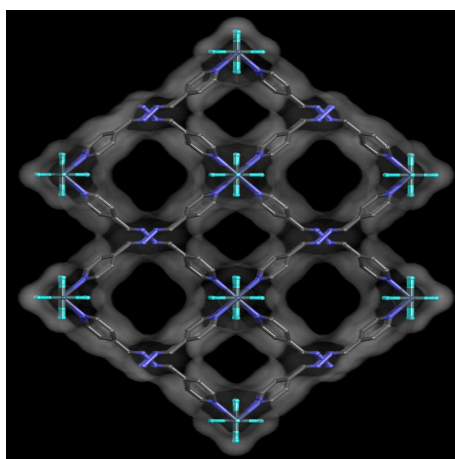


Figure 3. Packing diagram showing potential voids of framework. Color: Grey—C, Light Blue—N, Blue—Zn, Light green—Chlorine.

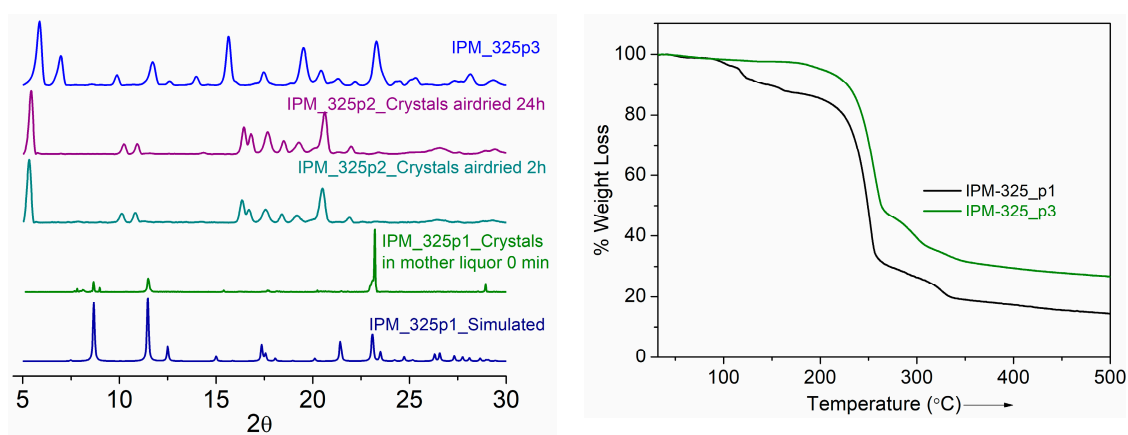


Figure 4. (a) Powder X-Ray diffraction patterns of simulated (IPM-325_p1) Color Code—Blue, IPM-325_p1_crystals soaked in mother liquor 0 min Color Code—Green, Air exposed after 2 h (IPM-325_p2) Color Code—Cyan, Air exposed after 24 h (IPM-325_p2) Color Code—Purple, Desolvated framework IPM_325_p3; (b) Thermogravimetric analysis of IPM-325_p1 and IPM-325_p3.

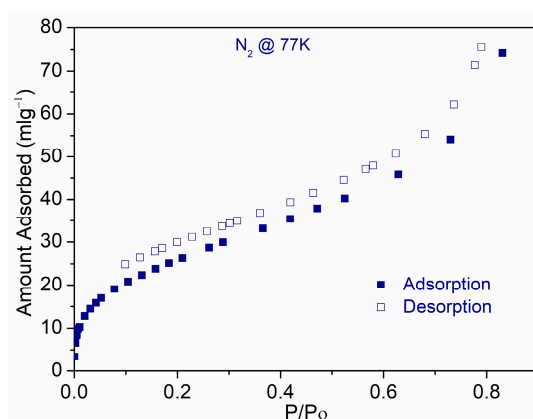


Figure 5. Low temperature nitrogen gas isotherm for IPM_325p3 at 77 K.

Table 1. Crystal data for IPM-325_p1.

Crystal Data	IPM_MOF-325-p1
Formula Crystal	{[Zn(L) ₂ (SiF ₆)]·(CH ₂ Cl ₂)·xG} _n Monoclinic
CCDC	1,586,047
a/Å	7.73 (9)
b/Å	20.36 (3)
c/Å	12.09 (14)
α/°	90
β/°	102.630 (2)
γ/°	90
Cell volume/Å ³	1857.6 (4)
Space group	C 2/m
Z	2
Dx/Mg m ⁻³	1.426
R	5.4

Acknowledgments: B.M. is thankful to CSIR for research funding. S.S. is thankful to IISER-Pune for research fellowship. We thank Aamod V. Desai for his inputs. We acknowledge IISER-Pune for research facilities. We would also like to acknowledge SERB (Project No. EMR/2016/000410) for generous financial support and DST-FIST (SR/FST/CSII-023/2012) for Single Crystal instrument facility.

Author Contributions: S.K.G. supervised the project. B.M. and S.S. carried out the experimentation and wrote the manuscript.

Conflicts of Interest: The authors declare no conflict of interest.

References

1. Furukawa, H.; Cordova, K.E.; O’Keeffe, M.; Yaghi, O.M. The chemistry and Applications of metal-organic frameworks. *Science* **2013**, *341*, 974. [[CrossRef](#)] [[PubMed](#)]
2. Ouay, B.L.; Kitagawa, S.; Uemura, T. Opening of an accessible microporosity in an otherwise nonporous metal-organic framework by polymeric guests. *J. Am. Chem. Soc.* **2017**, *139*, 7886–7892. [[CrossRef](#)] [[PubMed](#)]
3. Czaja, A.U.; Trukhan, N.; Muller, U. Industrial applications of metal-organic frameworks. *Chem. Soc. Rev.* **2009**, *38*, 1284–1293. [[CrossRef](#)] [[PubMed](#)]
4. Lustig, W.P.; Mukherjee, S.; Rudd, N.D.; Desai, A.V.; Li, J.; Ghosh, S.K. Metal-organic frameworks: Functional luminescent and photonic materials for sensing applications. *Chem. Soc. Rev.* **2017**, *46*, 3242–3285. [[CrossRef](#)] [[PubMed](#)]
5. Lee, J.; Farha, O.K.; Roberts, J.; Scheidt, K.A.; Nguyen, S.T.; Hupp, J.T. Metal-organic framework as catalysts. *Chem. Soc. Rev.* **2009**, *38*, 1450. [[CrossRef](#)] [[PubMed](#)]
6. Biswas, S.; Stock, N. Synthesis of metal-organic frameworks (MOFs): Routes to various MOF topologies, morphologies, and composites. *Chem. Rev.* **2012**, *112*, 933–969.
7. Zhou, H.-C.J.; Kitagawa, S. Metal-Organic Frameworks (MOFs). *Chem. Soc. Rev.* **2014**, *43*, 5415–5418. [[CrossRef](#)] [[PubMed](#)]
8. Lu, W.; Wei, Z.; Gu, Z.-Y.; Liu, T.-F.; Park, J.; Park, J.; Tian, J.; Zhang, M.; Zhang, Q.; Gentle, T., III; et al. Tuning the structure and function of metal-organic frameworks via linker design. *Chem. Soc. Rev.* **2014**, *43*, 5561–5593. [[CrossRef](#)] [[PubMed](#)]
9. Lalonde, M.; Bury, W.; Karagiari, O.; Brown, Z.; Hupp, J.T.; Farha, O.K. Transmetalation: Routes to metal exchange within metal-organic frameworks. *J. Mater. Chem. A* **2013**, *1*, 5453–5468. [[CrossRef](#)]
10. Brozek, C.K.; Dinca, M. Cation exchange at the secondary building units of metal-organic frameworks. *Chem. Soc. Rev.* **2014**, *43*, 5456–5467. [[CrossRef](#)] [[PubMed](#)]
11. Schoedel, A.; Li, M.; Li, D.; O’Keeffe, M.; Yaghi, O.M. Structures of metal-organic frameworks with rod secondary building units. *Chem. Rev.* **2016**, *116*, 12466–12535. [[CrossRef](#)] [[PubMed](#)]
12. Rimoldi, M.; Howarth, A.J.; DeStefano, M.R.; Lin, L.; Goswami, S.; Li, P.; Hupp, J.T.; Farha, O.K. Catalytic zirconium/hafnium-based metal-organic frameworks. *ACS Catal.* **2017**, *7*, 997–1014. [[CrossRef](#)]
13. Noro, S.-I.; Kitaura, R.; Kondo, M.; Kitagawa, S.; Ishii, T.; Matsuzaka, H.; Yamashita, M. Framework engineering by anions and porous functionalities of Cu(II)/4,4’-bpy coordination polymers. *J. Am. Chem. Soc.* **2002**, *124*, 2568–2583. [[CrossRef](#)] [[PubMed](#)]

14. Karmakar, A.; Desai, A.V.; Ghosh, S.K. Ionic metal-organic frameworks (iMOFs): Design principles and applications. *Coord. Chem. Rev.* **2016**, *307*, 313–341. [[CrossRef](#)]
15. Manna, B.; Desai, A.V.; Ghosh, S.K. Neutral N-donor ligand based flexible metal-organic frameworks. *Dalton Trans.* **2016**, *45*, 4060–4072. [[CrossRef](#)] [[PubMed](#)]
16. Eddaoudi, M.; Sava, D.F.; Eubank, J.F.; Adil, K.; Guillerm, V. Zeolite-like metal-organic frameworks (ZMOFs): Design, synthesis, and properties. *Chem. Soc. Rev.* **2015**, *44*, 228–249. [[CrossRef](#)] [[PubMed](#)]
17. Subramaniam, S.; Zaworotko, M.J. Porous solids by design: $[\text{Zn}(4,4'\text{-bpy})_2(\text{SiF}_6)]_n \times \text{DMF}$, a single framework octahedral coordination polymer with large square channels. *Angew. Chem. Int. Ed.* **1995**, *34*, 2127. [[CrossRef](#)]
18. Noro, S.-I.; Kitagawa, S.; Kondo, M.; Kenji, S. New methane adsorbent, porous coordination polymer, $[\text{Cu}(\text{SiF}_6)(4,4'\text{-bipyridine})_2]_n$. *Angew. Chem. Int. Ed.* **2000**, *39*, 2081–2084. [[CrossRef](#)]
19. Shekhah, O.; Belmabkhout, Y.; Chen, Z.; Guillerm, V.; Cairns, A.; Adil, K.; Eddaoudi, M. Made-to-order metal-organic frameworks for trace carbon dioxide removal and air capture. *Nat. Commun.* **2014**, *5*, 4228. [[CrossRef](#)] [[PubMed](#)]
20. Burd, S.D.; Ma, S.; Perman, J.A.; Sikora, B.J.; Snurr, R.Q.; Thallapally, P.K.; Tian, J.; Wojtas, L.; Zaworotko, M.J. Highly Selective Carbon Dioxide Uptake by $[\text{Cu}(\text{bpy-n})_2(\text{SiF}_6)]$ (bpy-1 = 4,4'-Bipyridine; bpy-2 = 1,2-Bis(4-pyridyl)ethene). *J. Am. Chem. Soc.* **2012**, *134*, 3663. [[CrossRef](#)] [[PubMed](#)]
21. Nugent, P.; Belmabkhout, Y.; Burd, S.D.; Cairns, A.J.; Luebke, R.; Forrest, K.; Pham, T.; Ma, S.; Space, B.; Wojtas, L.; et al. Porous materials with optimal adsorption thermodynamics and kinetics for CO_2 separation. *Nature* **2013**, *495*, 80–84. [[CrossRef](#)] [[PubMed](#)]
22. O'Nolan, D.; Kumar, A.; Zaworotko, M.J. Water Vapour Sorption in Hybrid Pillared Square Grid Materials. *J. Am. Chem. Soc.* **2017**, *139*, 8508–8513. [[CrossRef](#)] [[PubMed](#)]
23. Zhang, Z.; Yang, Q.; Cui, X.; Yang, L.; Bao, Z.; Ren, Q.; Xing, H. Sorting of C4 olefins with interpenetrated hybrid ultramicroporous materials by combining molecular recognition and size-sieving. *Angew. Chem. Int. Ed.* **2017**, *56*, 16282–16287. [[CrossRef](#)] [[PubMed](#)]
24. Schneemann, A.; Bon, V.; Schwedler, I.; Senkovska, I.; Kaskel, S.; Fischer, R.A. Flexible metal-organic frameworks. *Chem. Soc. Rev.* **2014**, *43*, 6062–6096. [[CrossRef](#)] [[PubMed](#)]
25. Chang, Z.; Yang, D.-H.; Xu, J.; Hu, T.-L.; Bu, X.-H. Flexible metal-organic frameworks: Recent advances and potential applications. *Adv. Mater.* **2015**, *27*, 5432–5441. [[CrossRef](#)] [[PubMed](#)]
26. Horike, S.; Shimomura, S.; Kitagawa, S. Soft porous crystals. *Nat. Chem.* **2009**, *1*, 695–704. [[CrossRef](#)] [[PubMed](#)]
27. Serre, C.; Millange, f.; Thouvenot, C.; Nogues, M.; Marsolier, G.; Louer, D.; Ferey, G. Very large breathing effect in the first nanoporous chromium(iii)-based solids: MIL-53 or $\text{Cr}^{\text{III}}(\text{OH}) \cdot (\text{O}_2\text{C}-\text{C}_6\text{H}_4-\text{CO}_2) \cdot \{\text{HO}_2\text{C}-\text{C}_6\text{H}_4-\text{CO}_2\text{H}\}_x \cdot \text{H}_2\text{O}_y$. *J. Am. Chem. Soc.* **2002**, *124*, 13519–13526. [[CrossRef](#)] [[PubMed](#)]
28. Hamon, L.; Llewellyn, P.L.; Devic, T.; Ghoufi, A.; Clet, G.; Guillerm, V.; Pirngruber, G.D.; Maurin, G.; Serre, S.; Driver, G.; et al. Co-adsorption and separation of CO_2 - CH_4 mixtures in the highly flexible MIL-53(Cr) MOF. *J. Am. Chem. Soc.* **2009**, *131*, 17490–17499. [[CrossRef](#)] [[PubMed](#)]
29. SAINT Plus, Version 7.03; Bruker AXS Inc.: Madison, WI, USA, 2004.
30. Krause, L.; Herbst-Irmer, R.; Sheldrick, G.M.; Stalke, D. Comparison of Silver and molybdenum microfocus X-ray sources for single crystal structure determination. *J. Appl. Cryst.* **2015**, *48*, 3–10. [[CrossRef](#)] [[PubMed](#)]
31. Sheldrick, G.M. A short history of SHELX. *Acta Crystallogr. Sect. A* **2008**, *64*, 112–122. [[CrossRef](#)] [[PubMed](#)]
32. Sheldrick, G.M. SHELXT—Integrated space-group and crystal-structure determination. *Acta Cryst.* **2015**, *C71*, 3–8. [[CrossRef](#)] [[PubMed](#)]
33. Farrugia, L. WinGX, version 1.80.05; University of Glasgow: Glasgow, Scotland, 2009.
34. Spek, A.L. PLATON SQUEEZE: A tool for the calculation of the disordered solvent contribution to the calculated structure factors. *Acta Cryst.* **2015**, *C71*, 9–18.
35. Bisht, K.K.; Suresh, E. Spontaneous Resolution to Absolute Chiral Induction: Pseudo-Kagome Type Homochiral Zn(II)/Co(II) Coordination Polymers with Achiral Precursors. *J. Am. Chem. Soc.* **2013**, *135*, 15690.

